ELSEVIER

Ceramics International 29 (2003) 599–609

CERAMICS INTERNATIONAL

www.elsevier.com/locate/ceramint

Thermal shock behaviour of mullite ceramic

M. Hamidouche[a,*], N. Bouaouadja[a], C. Olagnon[b], G. Fantozzi[b]

[a]*Laboratoire des Matériaux Non Métalliques, Département d'O.M.P., Faculté des Sciences de l'Ingénieur, Université de Sétif—19000, Algeria*

[b]*Laboratoire GEMPPM, URA 341, INSA de Lyon, 69621 Villeurbanne Cedex, France*

Received 4 January 2001; received in revised form 8 August 2002; accepted 10 September 2002

Abstract

The aim of this work is to study some aspects of the thermal shock of mullite ceramic. Mullite samples are submitted to mild thermal shock by quenching in a compressed air flow using a Biot number $\beta = 0.3$. The cooling duration is 6 s with a superficial heat exchange coefficient $h = 600$ W/m^2°C. This duration is sufficient for the transient thermal stress to reach its maximal value. The critical temperature difference ΔT_C found equal to 750 °C was obtained by measuring the retained mechanical strength and the Young's modulus. For determining the failure time and $\Delta T_{C,}$ we used the acoustic emission technique. Finally, the thermal shock experiments are modelled by a two dimensional cooling model, allowing a precise determination of the induced stress intensity factor K_I.

Keywords: C. Thermal properties; C. Toughening; D. Mullite; Numerical simulation

1. Introduction

The mullite ceramic has had and will continue to have a significant role in the development of traditional and advanced ceramics. Mullite is the only stable crystalline phase in the aluminosilicate system, under normal atmospheric pressure at room through elevated temperatures [1]. Its chemical composition ranges from $3Al_2O_3$–$2SiO_2$ to approximately $2Al_2O_3$–SiO_2. The incongruous melting behaviour of mullite is now widely accepted [2]. It has received significant attention during the last decade as a potential structural material for high temperature applications [3,4].

Mullite exhibits high refractoriness, low creep rate [5], low thermal expansion, low thermal conductivity [6], good chemical and thermal stability [7] and average fracture toughness and strength [8]. The presence and the distribution of remaining glassy phases caused by impurity contents along grain boundaries or forming isolated pockets will influence the mechanical behaviour at high temperature [9].

During a sudden temperature change of a body, there occurs transient temperature distributions which induce thermal stresses. This results in so-called 'thermal shock' when the body is made suddenly in contact with an environment at different temperature. The shock intensity is related to the temperature difference level between the initial body temperature and that of the environment. There is a distinction between an ascending thermal shock and descending one. The later one is more harmful to brittle materials as it generates tensile stresses on the surface. In addition, the lower thermal conductivity of the structural ceramics at high temperature increases the Biot number. As a consequence, the induced thermal stresses become more important. These parameters may be sufficient to activate pre-existing micro-cracks and to lead to material damage or fracture.

One of the earliest analysis in the ceramics literature was proposed by Kingery [10]. The thermal shock theory has been progressively refined by numerous authors during the last 40 years [11–13]. The different analysis always start with the evaluation of the temperature in the transient mode, following the stress computations. The oldest works used analysises that are often complex for a simple geometrical case. As a consequence, a number of parameters characterizing the thermal shock

* Corresponding author.

0272-8842/03/$30.00
doi:10.1016/S0272-8842(02)00207-9

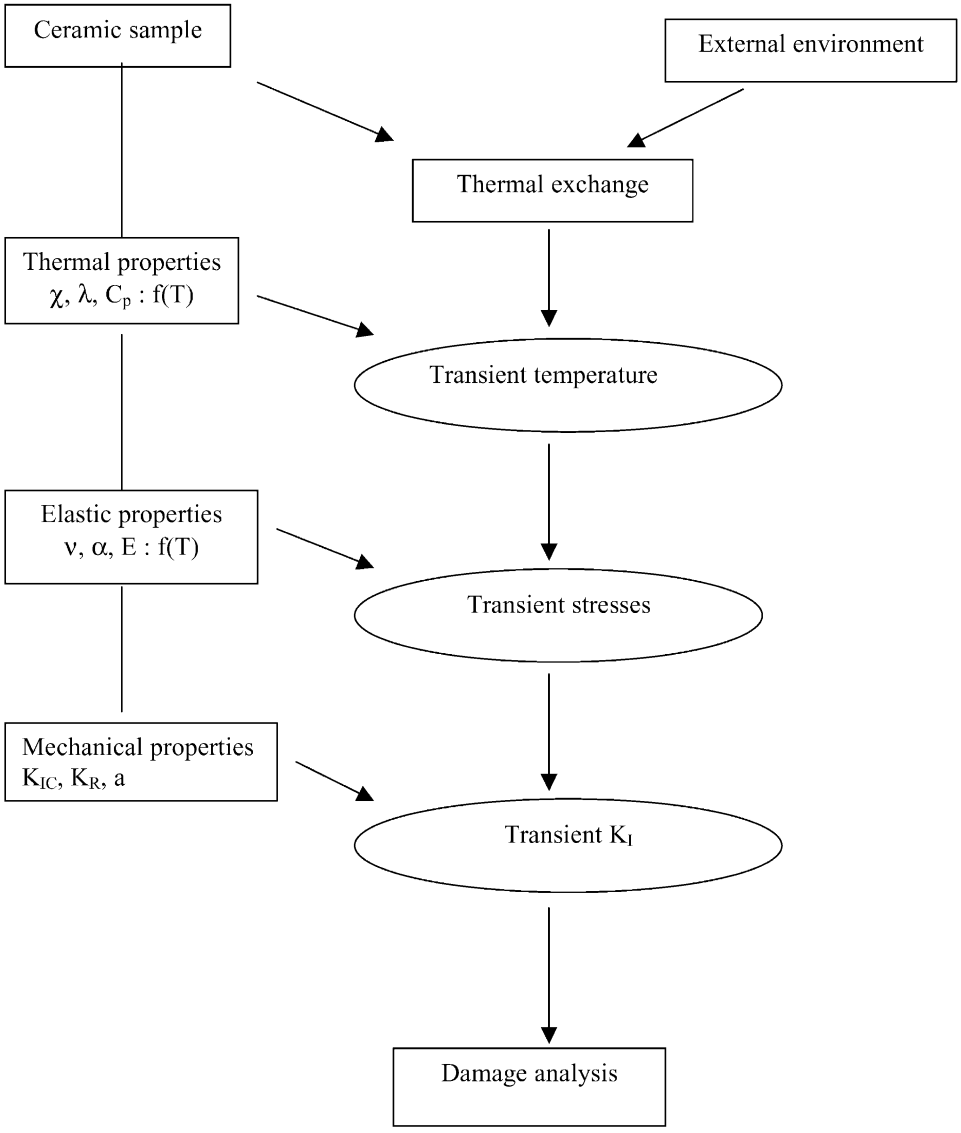

Fig. 1. Diagram showing the three transitory stages of the thermal shock.

were introduced. More recently [14], fracture mechanics principles were introduced. The intensity factor K_I for a geometrical case is evaluated and is compared to the fracture characteristics of the material (Fig. 1). The recent development of numerical methods has helped to apply these theories to complex forms by taking into account the temperature dependence on the material properties.

Experimental methods for determining thermal shock damage are numerous. There are static methods [15] for measuring the weight loss and the mechanical strength deterioration. Other dynamic methods [16] control the damage by measuring the frequency disturbances and the stationary or moving waves damping caused by the thermal shock.

The aim of this work is to study the thermal shock behaviour of a sintered mullite.

2. Experimental procedure

2.1. Material

The material used was made from a commercial mullite powder (Baikowski 193 CR France). This powder was first ball-milled during 2 h until an average particle size of 0.7 μm using mullite balls (1–2 mm diameter) and containers with isopropyl alcohol as milling medium. This powder was isopressed at 200 MPa into blocks of dimensions $50\times50\times10$ mm^3. They were subsequently heat treated at 1750 °C during 5 h. During the cooling process, the samples were maintained at 1450 °C during 5 h. This step is necessary for reducing the vitreous phase quantity. Rectangular samples with dimensions $40\times6\times4$ mm^3 were prepared from these blocks for the different mechanical tests. The sides of these samples

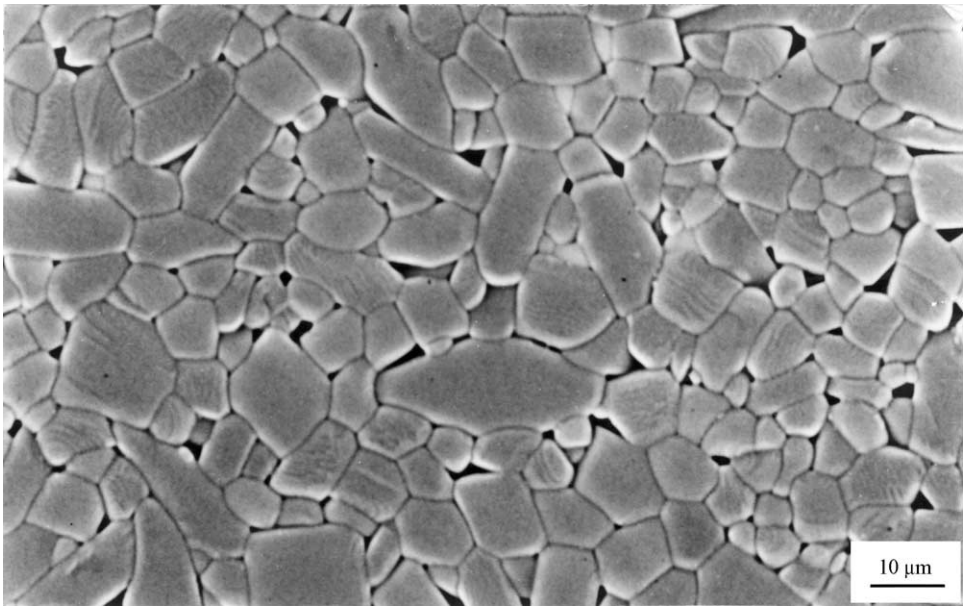

Fig. 2. Micrograph showing the microstructure of mullite.

submitted to tension during the flexural tests were polished with 1 μm diamond paste. The polished bars were annealed during 2 h at 1200 °C.

2.1.1. Microstructure

The microstructure was observed by SEM after thermal etching. Typical micrograph of etched surface is shown in Fig. 2. We can see two kinds of grains corresponding to a matrix with equiaxed grains and whose average lengths are in the range 5–10 μm and a second distribution of acicular grains with an average size range of 15–25 μm. These acicular grains have a homogeneous distribution and a random orientation. Cavities of about 1 μm are present in some triple points.

2.1.2. Main material characteristics

The main characteristics of the tested material, measured at ambient temperature, are gathered in Table 1.

2.1.3. Temperature dependent properties

Some mullite properties as a function of temperature were measured. To study thermal expansion, a test was carried out from ambient temperature to 1000 °C in a silica sample holder dilatometer. The coefficient of thermal expansion over the range of temperature from 25 to 1000 °C was fitted to a polynomial:

$$\alpha_M(T) = -10^{-17}T^4 + 4.10^{-14}T^3 - 4.10^{-11}T^2 + 2.10^{-8}T + 7.10^{-7} \ (^\circ C^{-1}) \quad (1)$$

where T is the absolute temperature.

Young's modulus, E, was measured as a function of temperature by the resonance frequency in bending:

$$E_M(T) = -0.0157T + 203.8 \ \text{(GPa)} \quad (2)$$

Thermal conductivity was obtained from the literature.[17] In the range from 20 to 800 °C it can be fitted by:

$$\lambda_M(T) = 10^{-17}T^6 - 6.10^{-14}T^5 + 8.10 - 11T^4 - 5.10^{-8}T^3 + 10^{-5}T^2 - 0.0022T + 5.165 \ \text{(W/m K)} \quad (3)$$

The specific heat Cp was also derived from the literature[17] since it is mostly dependent on the chemical composition:

$$Cp_M(T) = 2.10^{-14}T^6 - 8.10^{-7}T^5 + 10^{-7}T^4 - 10^{-4}T^3 + 0.7T^2 - 17.09T + 2456 \ \text{(J/kg K)} \quad (4)$$

Since the Poisson's ratio is generally weakly dependent on the temperature, it was only measured at room temperature only by the wave velocity method which yielded: $\nu = 0.28$.

Table 1
Main material characteristics at ambient temperature

Characteristics	Values	Method used
Mechanical strength (MPa)	254±20	Four points bending
Young modulus (GPa)	214	Resonance frequency
Fracture toughness (MPa$\sqrt{m}$)	2.4±0.15	SENB
Density (g/cm^3)	3.08	Archimede's
Poisson's ratio	0.28	Ultrasonic

2.2. Thermal shock test apparatus

To heat samples at different initial temperatures, we used a furnace that can reach a temperature of 1400 °C

in air. The samples were cooled by a compressed air jet at a pressure of 4 bars at ambient temperature. A sample holder allows the sample displacement between the cold and the hot regions through the medium of a pneumatic jack. The acoustic activity reception by means of a piezo-electrical sensor is attached to this sample holder. The wave-guide is characterised by a good resistance to thermal shock, thermal fatigue and oxidation. Besides, it doesn't present any phase transformation at working temperatures that can disturb the acoustic emission. The acoustic and thermal insulator is made of an alumino-silicate ceramics. Two thermocouples are used for measuring the sample (where was the thermocouple attached) and kiln temperatures. The acoustic activity and the control handling are made through a microcomputer.

2.3. Thermal shock test procedure

The test made is a descendant thermal shock test type. Its severity is expressed in term of the Biot number β ($\beta = a.h/k = 0.3$). We used a heat transfer coefficient $h = 600$ W/m^2 °C. The specimen half-thickness $a = 2$ mm and the thermal conductivity of mullite $\lambda = 5$ W/m K. The sample is maintained at the higher temperature during six minutes for making the temperature uniform. The sample transportation to the cold zone takes approximately three seconds. The cooling process lasts 6 s. This duration is insufficient to obtain the thermal equilibrium, but the maximal temperature difference between the surface and the centre of the specimen is reached. So, the maximal transient thermal stress in the sample is obtained before this cooling duration (6 s). The acoustic activity is recorded during the thermal shock. Strength measurements were made after the thermal shock tests using a four point loading configuration with an inner and an outer span with a 10 and 35 mm, respectively. The tests were carried out in air using an Instron testing machine with a crosshead speed of 0.5 mm/min. Young's modulus was measured by the resonance frequency method using a Grindo-Sonic type apparatus.

2.4. Finite element modelling

The modelling is based on the local approach of the thermal shock. The model used is presented in Fig. 3. A 2D cross section of a rectangular beam was modelled. Because of symmetry, we concentrated on one sample quarter. We began by determining the transient temperature distribution. We then evaluate the transient surface stresses and finally the stress intensity factor K_I using the principle of superposition [14]. We integrated in this numerical procedure the temperature dependence of the mullite thermo-elastic properties. The heat transfer coefficient h was taken as determined in a previous work [18]. It is important to point out that the frontal and lateral heat transfer are identical and remain independent of temperature [$h = h_f = h_l = 600$ W/(m^2 °C)]. We used a software package (ABAQUS) based on finite element analysis. It enables to evaluate bidimensionally the temperatures and the stresses at every instant of the thermal shock and at every point on the sample.

In our case, by referring to our experimental results (acoustical emission, Young's modulus and mechanical strength after damage), the computations were oriented to particular cases. We were especially interested to fracture initiation moments during the cooling process and to the crack initiation site (near the centre of the 40×6 mm^2 sample surface).

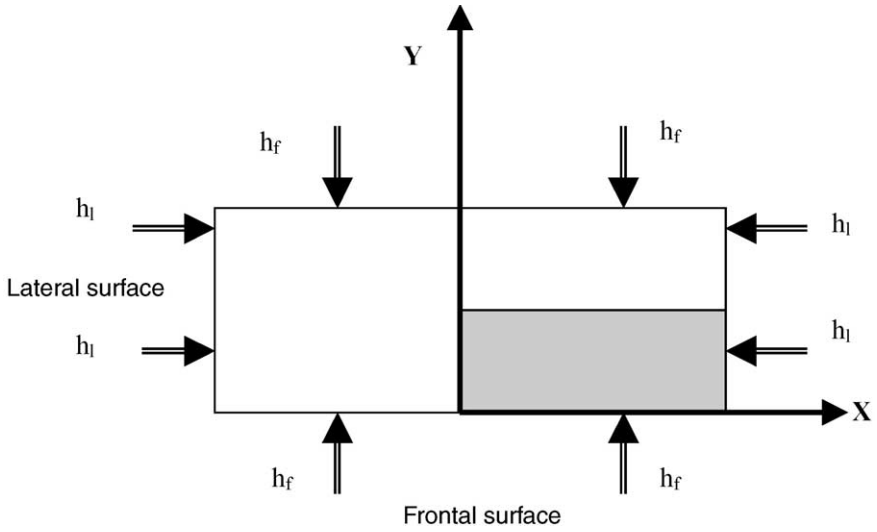

Fig. 3. Illustration of heat transfer model (h_f: frontal surface heat coefficient, h_l: lateral surface heat coefficient).

3. Results and discussion

3.1. Thermal shock results

Relative strength (σ/σ_0) and relative Young's modulus (E/E_0) represent values obtained after damage and normalised to the initial values. Fig. 4 shows that the mechanical relative strength remains constant up to a temperature difference of 750 °C. Beyond this limit, it decreases sharply. This rapid strength variation indicates the critical temperature difference causing material damage. This temperature difference corresponds to the propagation of a single longitudinal crack observed at the centre of the frontal face of the tested specimen. From these results, we notice that this technique can still be used to characterise the critical temperature difference ($\Delta T_C = 750$ °C). Above this point some strength scattering can be observed. It is related to the statistical distribution of the cracks induced by thermal shock (size and position distributions). The relative strength is about 60% for a cold air quench at temperature difference (ΔT) of 900 °C. This shows that mullite has a fairly good thermal shock damage resistance.

On the other hand, Fig. 5 shows that the Young's modulus variation is rather smooth (without any sudden

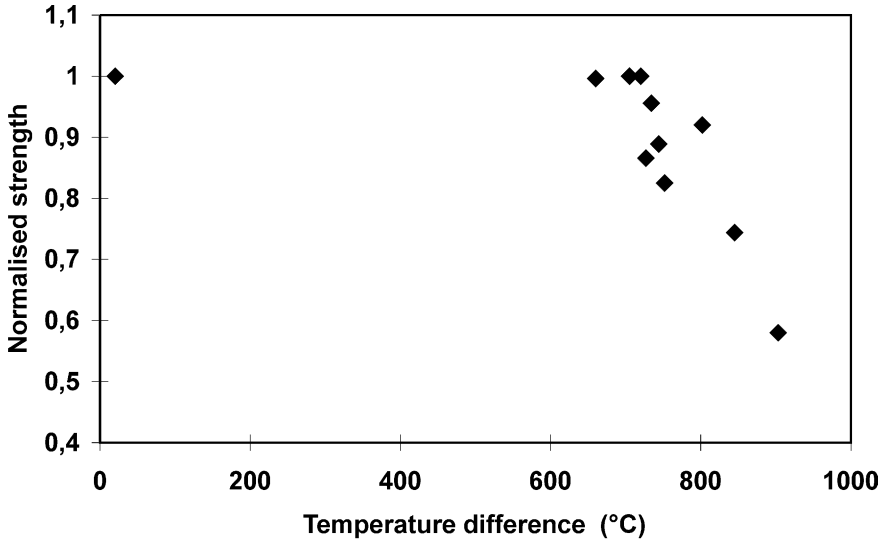

Fig. 4. Dependence of the relative strength behaviour of mullite ceramic samples subjected to thermal shock by a cold air quench on temperature difference ΔT.

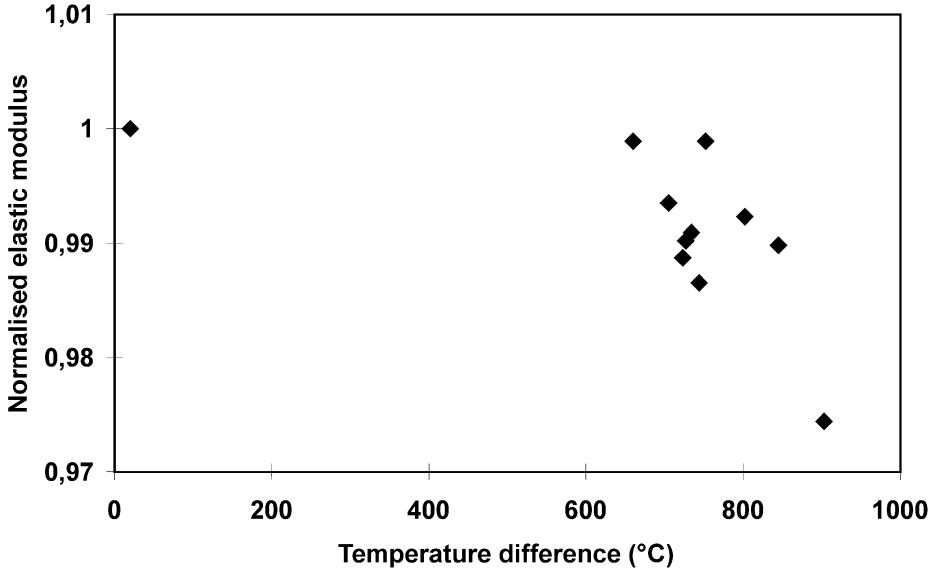

Fig. 5. Dependence of the relative Young's modulus behaviour of mullite ceramic samples subjected to thermal shock by a cold air quench on temperature difference ΔT.

change) comparing to the strength variation case. There is a regular and less pronounced decrease. Therefore, precise critical temperature difference cannot be predicted from Young's modulus results because it is more sensitive to defects in the sample volume.

Fig. 6 shows an example of acoustic emission registered during the thermal shock (6 s) for a critical temperature difference ($\Delta T_c = 750$ °C) and two sub-critical temperature differences ($\Delta T = 850$ °C and $\Delta T = 900$ °C). It is evident that the number, the amplitude and the

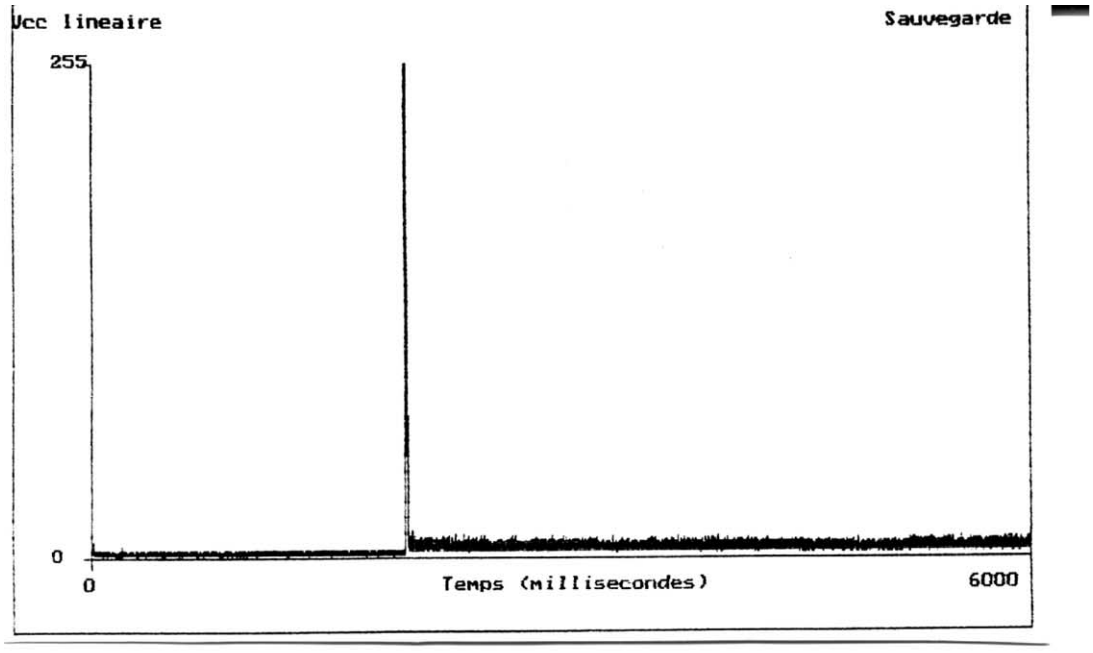

a) ΔTc = 750°C , Events number = 1, initial time ti = 2000 µs

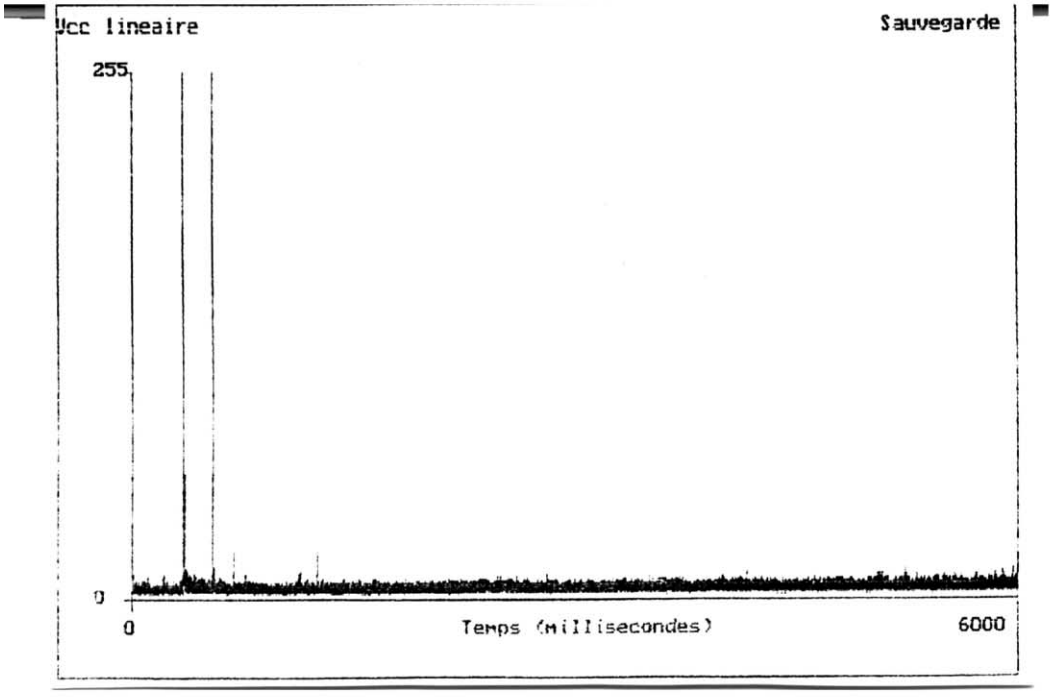

b) ΔT_C = 850°C , Events number = 4, initial time ti = 350 µs

Fig. 6. Acoustic emission activity registered for mullite samples thermally shocked by air at three temperature differences ($\Delta T = 750$ °C, $\Delta T = 850$ °C and $\Delta T = 900$ °C) during 6 s.

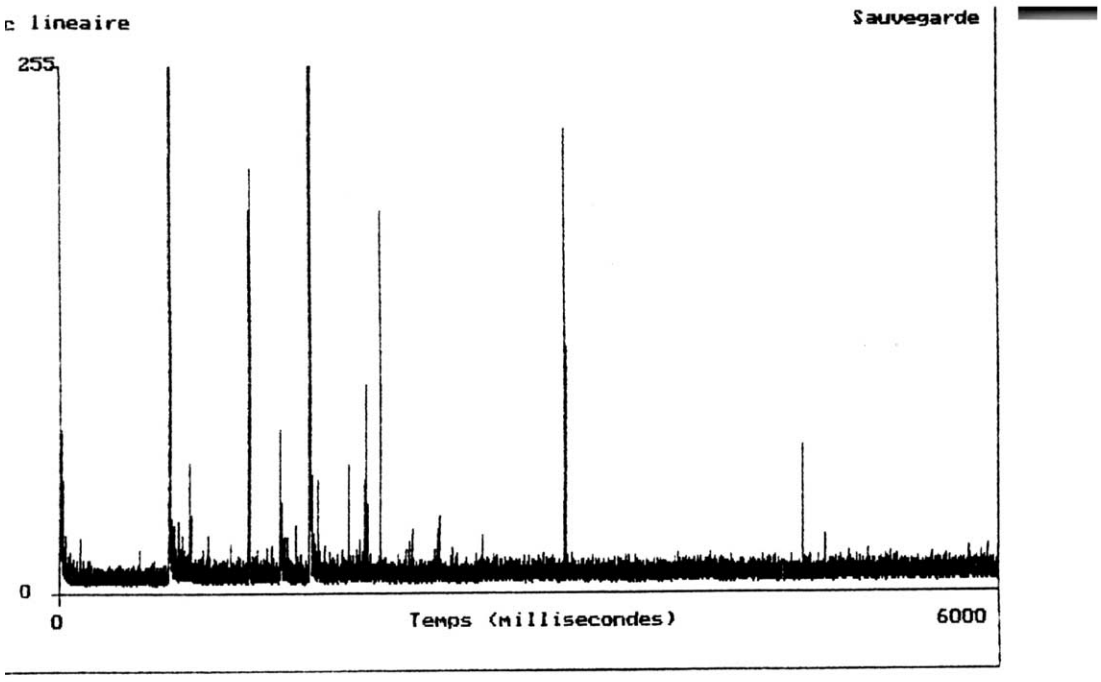

Fig. 6 (*continued*).

acoustic emission initiation time are very sensitive to the fixed temperature difference. This emission occurs for temperature difference greater than 750 °C. This results shows that the acoustic emission control is in good accordance with the strength results. Beyond the critical temperature, the acoustic emission is maximum (Fig. 6b), corresponding to a catastrophic cracking type.

It clearly appears that when the shock severity increases, the emitted acoustic event number becomes more important. This relation is governed by the released energy for creating new surfaces during the propagation of the most critical flaw. The events number can then be related to the crack dimensions (length and depth) induced by the thermal shock. Fig. 7 confirms the existing relation between the initial thermal shock temperature and the acoustic events number. We can notice that the emission initial time of the first event is directly related to the temperature difference of the thermal shock (Fig. 8). Indeed, when the temperature difference is important, the generated stresses become more important leading therefore to a precocious early cracking occurring at the start of the cooling process.

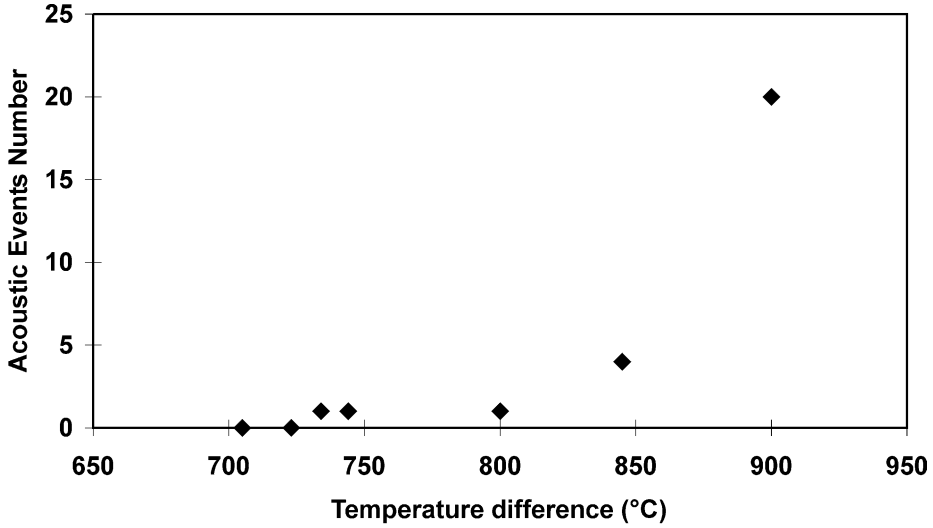

Fig. 7. Evolution of acoustic events number with thermal shock temperature difference ΔT for mullite samples cooled by air jet during 6 s.

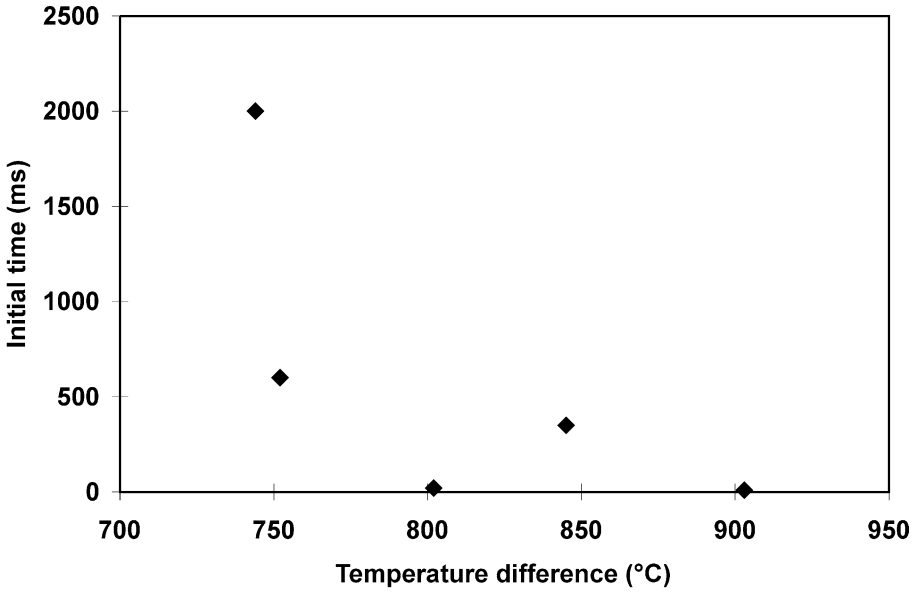

Fig. 8. Acoustical emission initiating time versus temperature difference ΔT for thermally shocked mullite ceramic ($\beta = 0.3$).

The thermally shocked samples observation (by dye penetrant) shows that there is a unique crack. It propagates through the sample in the longitudinal direction and then bifurcating toward the lateral sides. This crack deviation is caused by the stresses generated in the region in contact with metallic sample holder. The heat transfer in this case will be different than the one taking place in the middle of the sample where the shock is more severe. No crack branching or secondary cracks were observed in any tested sample.

3.2. Modelling

During the experimental tests made on mullite, we noticed that at the critical temperature difference $\Delta T_C = 750$ °C, the cracking is unique and longitudinal. It occurs at the centre of the frontal sample surface. For this purpose, the computations were oriented to this situation.

3.2.1. Transient temperature

We made the transient temperatures computations at the instant and at the site where the crack appears. We noticed, during experimental tests, that the damage starts at the critical temperature difference of 750 °C and it lasts at a cooling time of 1.428 s. The acoustical emission characterising the material damage occurred at this particular instant ($t = 1.428$ s) of the critical thermal shock.

We therefore limited our work to these critical thermal shock conditions leading to the crack propagation in the mullite material. At the critical instant ($t_c = 1.428$ s), the sample surface temperature is 598 °C, whereas that of the sample centre is at 680 °C. We determined the transient temperature difference between the surface and the sample centre for any instant during the cooling process for a thermal shock starting at the temperature of 750 °C. The maximal temperature difference ($T_c - T_s$) is about 82 °C after a cooling time of 1.428 s (Fig. 9).

3.2.2. Transient thermal stresses

Using transient temperatures, we numerically computed by finite elements analysis the transitory stresses using linear elasticity equations. In the computations, we integrated the temperature dependence of the mullite elastic properties as the crack appears. The maximum tensile stress is obtained on the largest face of the specimen, precisely in the middle of this face where the first crack propagation was observed. In this situation, only the principal tensile stresses $\sigma_{xx}(y, t)$ along the line $x = 0$ which generates an opening mode for the first propagated crack will be taken into account.

Fig. 10 represents the transient stresses evolution $\sigma_{xx}(0, t)$ at the surface for the critical thermal shock. This superficial stress reaches its maximum (122 MPa) after a cooling time of 1.428 s, corresponding to the first cracks appearance moment revealed by acoustical emission.

The stress σ_{xx} variation versus the sample depth at the same instant ($t = 1.428$ s) is given in Fig. 11. We notice that the maximum stress (122 MPa) occurs at the surface. The stresses induced are of tensile type up to a depth of 0.8 mm representing one fifth of the sample thickness. They become compressive beyond this limit. The compressive stress reaches a value of 60 MPa in the centre of the sample. This is about half the surface tensile stress.

3.2.3. Stress intensity factor

During a thermal shock, a critical superficial flaw will propagate in surface and in depth directions. The stress intensity factor was evaluated with the hypothesis of a

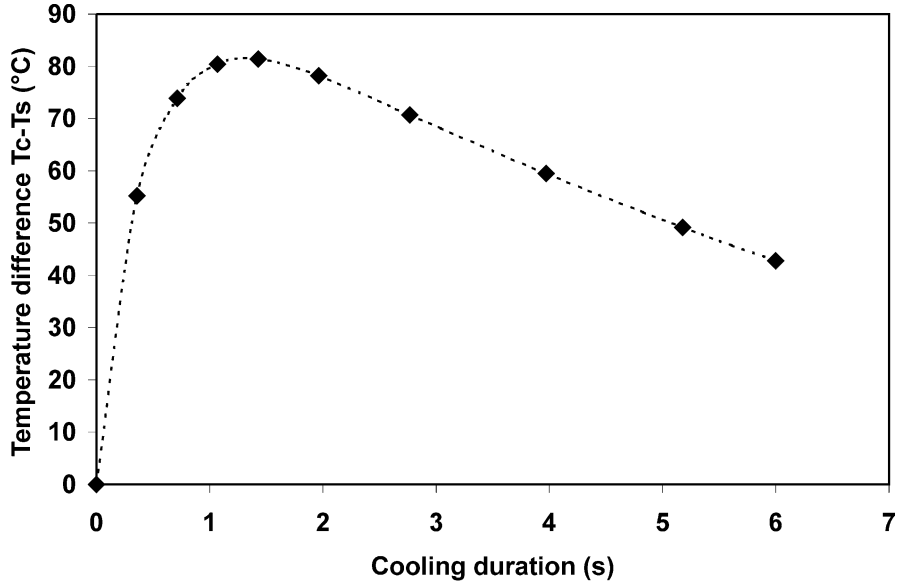

Fig. 9. Centre-surface temperature difference ($T_c - T_s$) variation versus cooling duration in the case of a critical thermal shock ($\Delta T_c = 750$ °C) for mullite for a Biot number $\beta = 0.3$.

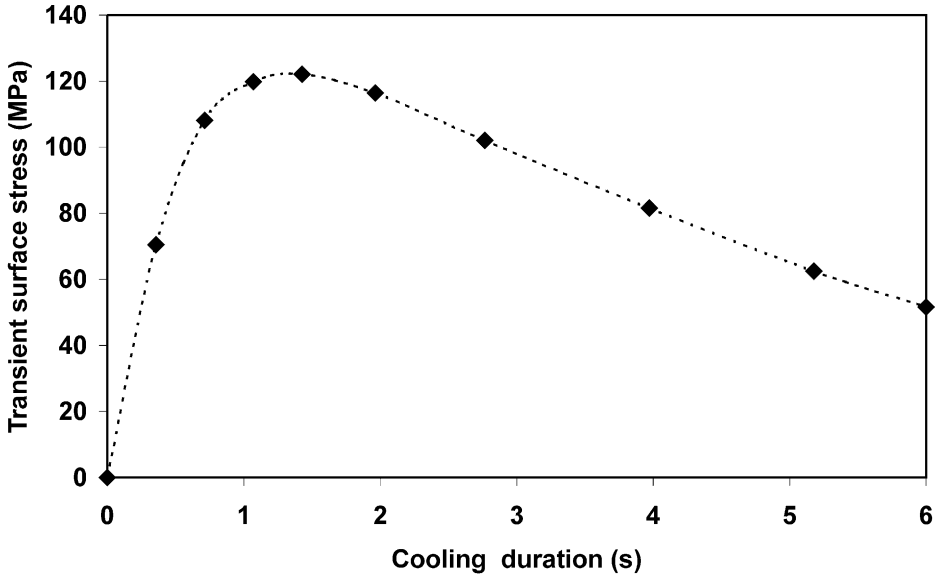

Fig. 10. Transient surface stress σ_{xx} (calculated with the transient temperature in Fig. 9) versus cooling duration of mullite shocked by air at $\Delta T = 750$ °C.

unidirectional crack propagation submitted to the stress profile $\sigma_{xx}(y, t)$ according to Wu's calculation [18]. The K_I was computed considering a semi-circular surface crack located at the centre of the frontal surface. In this case, the stress intensity factor corresponding at the deepest point runs above the stress intensity factor corresponding at the surface point at any cooling time. In Fig. 12, we represented the stress intensity factor $K(a, t)$ variations with the crack depth for the transient stress distributions showed in Fig. 11. The envelope of the curves has a maximum at the time $t = 1.428$ s. The stress intensity factor $K(a, t)$ is greater than the critical value K_{IC} for that time and a flaw size of 80 μm. This critical flaw size was determined according to the relation:

$$K_{IC} = \sigma_r . y . \sqrt{a_c} \quad (5)$$

y is the shape factor, σ_r the fracture strength of the material, a_c the critical flaw size, K_{IC} the fracture toughness.

The critical flaw size a_c was determined using the temperature of 600 °C corresponding to the surface temperature at the time 1.428 s. At the end of the thermal

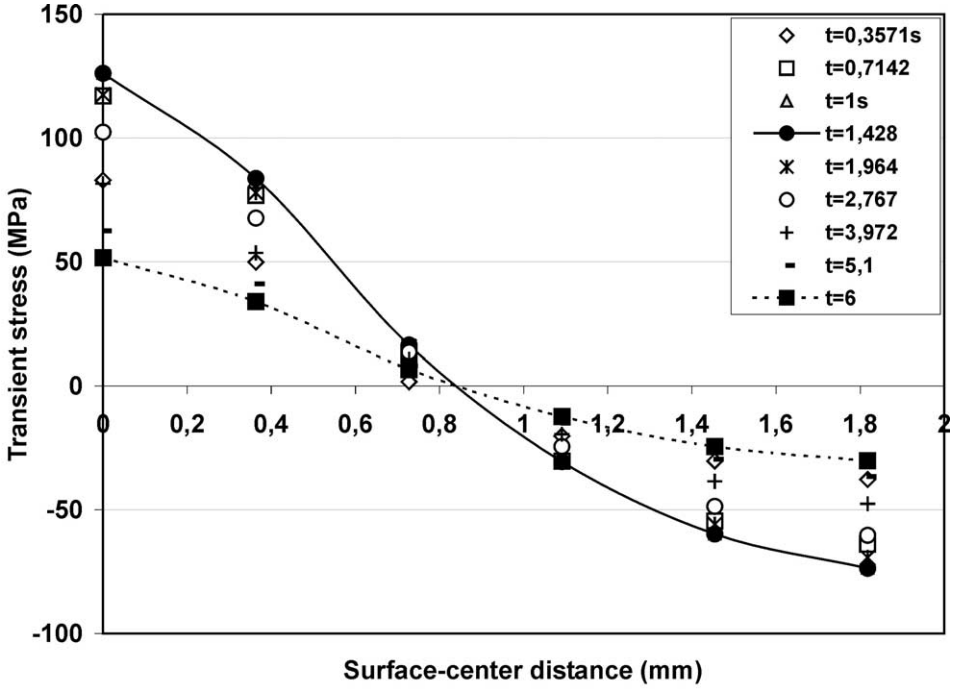

Fig. 11. Normal transient stresses σ_{xx} (at the plane $x=0$) distribution in depth direction surface-centre at different cooling times for mullite shocked at $\Delta T=750$ °C.

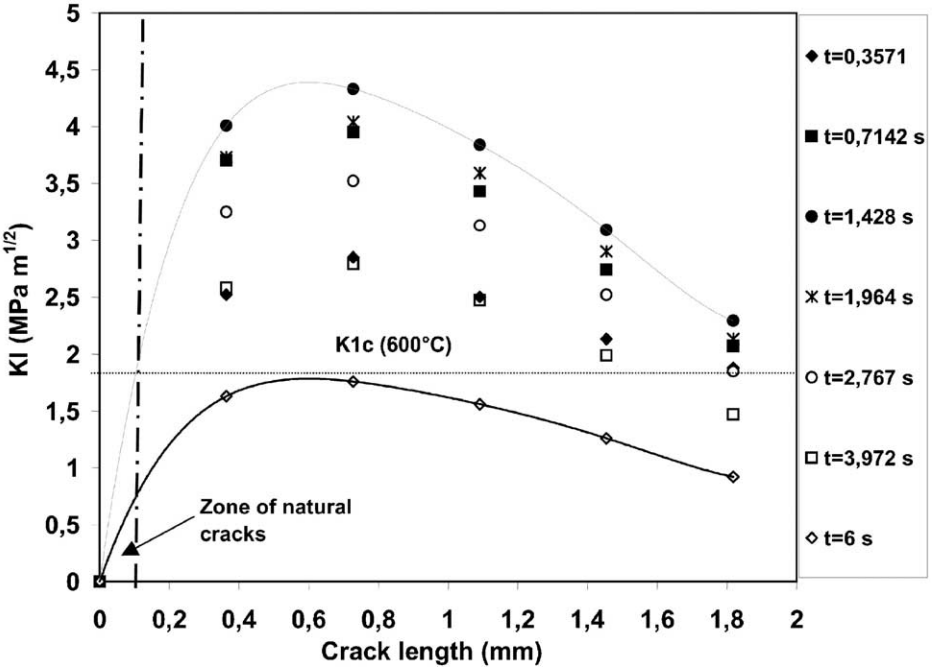

Fig. 12. Critical thermal shock ($\Delta T=750$ °C) generated stress intensity factor K_I of mullite ceramics versus crack length for a Biot number of 0.3 and a range of cooling time.

shock, a flaw of 80 μm size will reach a final length a_f corresponding to 1750 μm. Such a flaw size will induce fracture at a stress of 50 MPa, representing about 20% of the initial stress ($\sigma_r=254$ MPa). The experimental results showed that the critical thermal shock would reduce the initial strength to about 25%. The difference is probably related to the cracking mode. As the critical thermal shock induces only one crack through the sample, we used in this study the opening mode for the determination of the critical flaw size.

Knowing that there are no toughening mechanisms in mullite (microcracking, transformation toughening, crack bridging...), the stress intensity factor remains the only criterion for characterising the thermal damage.

4. Conclusion

- Mullite presents a critical temperature difference ΔT_C of about 750 °C in the case of cooling thermal shock with: Biot number $\beta = 0.3$, heat transfer coefficient $h = 600$ W/m^2 °C and specimen size of $(40 \times 6 \times 4)$ mm^3.
- The thermal shock damage control by acoustic emission leads to results similar to those obtained by measuring the residual strength or the elastic modulus after the shock.
- The number of acoustic events increases while the emission onset time decreases with increasing shock severity.
- The thermal shock simulation by the local approach corresponds to the experimental results.
- The stress intensity factor allows a better thermal shock prediction than the stress calculation.

References

[1] Y.L.A. Aksa, et al., Mullite for structural, electronic and optical applications, J. Am. Ceram. Soc. 74 (10) (1991) 2343–2358.
[2] A.J. Skoog, et al., Refractory of the past for the future: mullite and its use as a high bonding phase, Ceram. Bull. 67 (7) (1988) 1180–1185.
[3] G. Orange, et al., High temperature mechanical properties of reaction sintered mullite–zirconia composites and mullite–alumina–zirconia composites, J. Mater. Sci. 20 (1985) 2533–2540.
[4] M. Hamidouche, et al., Thermomechanical behaviour of mullite–zirconia composite, J. Eur. Ceram. Soc. 16 (1996) 441–445.
[5] P.A. Lessing, et al., Creep of polycrystalline mullite, J. Am. Ceram. Soc. 58 (3/4) (1975) 149–153.
[6] H. Schneider, et al., Thermal expansion of mullite, J. Am. Ceram. Soc. 37 (7) (1990) 2073–2076.
[7] R.F. Davis, Decomposition of mullite, J. Am. Ceram. Soc. 55 (2) (1972) 98–101.
[8] S. Kanaki, et al. Mechanical properties of pressureless sintered mullite ceramics, in: 2nd Int. Symp. of Ceram. Mater. and Components for Engines, Lubeck-Travemunde, Germany, 14–17 April 1986, pp. 625–631.
[9] M.I. Osendi, et al., Mechanical properties of mullite materials, J. Eur. Ceram. Soc. 16 (1996) 217–224.
[10] W.D. Kingery, Factors affecting thermal stress resistance of ceramic materials, J. Am. Ceram. Soc. 38 (1) (1955) 3–15.
[11] D.P.H. Hasselman, Unified theory of thermal shock fracture initiation and crack propagation in brittle ceramics, J. Am. Ceram. Soc. 52 (11) (1969) 600–604.
[12] A.G. Evans, Thermal shock fracture in ceramic materials, Proc. Br. Ceram. Soc. 25 (1975) 217–235.
[13] G.A. Schneider, Thermal shock criteria for ceramics, Ceram. Int. 17 (1991) 325–333.
[14] X.R. Wu, Application of weight function method for crack analysis in thermal stress field, in: G. A. Shneider (Ed.), Thermal shock and thermal fatigue behaviour of advanced ceramics, 8–13 November 1992, schloβ Ringberg, Germany, Academic, Germany, 1992.
[15] D.R. Larson, J.A. Coppola, D.P.H. Hasselman, Fracture toughness and spalling behavior of high Al_2O_3 refractories, J. Am. Ceram. Soc. 57 (10) (1974) 417–421.
[16] J.C. Glandus, Rupture fragile et résistance aux chocs thermiques de céramiques à usage mécanique, Doctorat Thesis, ENSCI, Limoges, 1981.
[17] H. Schneider, et al., Mullite and Mullite Ceramics, John Wiley & Sons, Chichester, 1994, 251..
[18] F. Mignard, C. Olagnon, G. Fantozzi, Acoustic emission monitoring of damage evaluation in ceramics submitted to thermal shock, J. Eur. Ceram. Soc. 15 (1995) 651–653.